

Article

Molecular Docking of Active Compounds from The Ethanol Extract of *Phaleria macrocarpa* Fruit with Iron Transporters DMT1 and ZIP14

Article Info

Article history :

Received May 09, 2024
Revised May 30, 2024
Accepted June 06, 2024
Published June 30, 2024

Keywords :

Molecular docking,
Phaleria macrocarpa,
DMT-1, ZIP-14,
Iron overload

Rahma¹, Ari Estuningtyas^{2*}

¹Master's Programme in Biomedical Sciences, Faculty of Medicine, Universitas Indonesia, Jakarta, Indonesia

²Department of Pharmacology and Therapeutics, Faculty of Medicine, Universitas Indonesia, Jakarta, Indonesia

Abstract. Iron-overload can lead to organ damage by promoting free radical production. This study explores the potential inhibitory effects of compounds found in *Phaleria macrocarpa* fruit on non-transferrin-bound iron uptake by targeting DMT1 and ZIP14 iron transporters through in-silico methods. The study utilized homology modeling to construct 3D structures of DMT1 and ZIP14. Validation of these models was carried out by assessing their sequence identity and analyzing their stereochemical quality using Ramachandran plots. Molecular docking was conducted using AutoDockTools. The coordinates for molecular docking were carefully chosen based on the iron binding-site locations as reported in previous literature. Interaction visualization was done using LigPlot+. Our findings indicate strong binding affinities of several compounds from *Phaleria macrocarpa* fruit with both DMT1 and ZIP14. Specifically, patuletin-7-O-[6''-(2-methylbutyryl)]-glucoside, naringenin-4'-7-dimethyl ether, and 5,7,8,3',4'-pentamethoxyflavone demonstrated significant interaction with DMT-1, while 6'-O-galloyl-homoarbutin, patuletin-7-O-[6''-(2-methylbutyryl)]-glucoside, and guanine exhibited high affinity for ZIP14. While the ethanol extract of *Phaleria macrocarpa* fruit shows promising interactions with key iron transporters implicated in iron overload, these in-silico predictions require further experimental validation to confirm their efficacy as inhibitors.

This is an open access article under the [CC-BY](https://creativecommons.org/licenses/by/4.0/) license.



This is an open access article distributed under the Creative Commons 4.0 Attribution License, which permits unrestricted use, distribution, and reproduction in any medium, provided the original work is properly cited. ©2024 by author.

Corresponding Author :

Ari Estuningtyas

Department of Pharmacology and Therapeutics, Faculty of Medicine,
Universitas Indonesia, Jakarta, Indonesia

Email : ari.estuningtyas@ui.ac.id

1. Introduction

Iron is a critical mineral indispensable for myriad physiological processes in the human body, including, but not limited to, oxygen transport, energy production, as well as DNA synthesis and repair processes [1-2]. Not only iron deficiency can disrupt health, but also iron excess has been shown to cause damage to various organs, such as the heart and blood vessels, liver, and hematological system [3-4]. Iron overload conditions like this are common in patients with thalassemia and represent one of the main causes of mortality and poorer survival in these individuals [5-6]. In cases of thalassemia, iron overload occurs due to repeated blood transfusions and increased iron absorption in the intestine as compensation for ineffective erythropoiesis. On the other hand, the body lacks physiological mechanisms to excrete this excess iron, allowing its accumulation [7].

Both the function and toxicity of iron are related to its ability to participate in oxidation and reduction reactions, converting between the Fe^{2+} and Fe^{3+} forms [2][8]. Under normal physiological conditions, iron is not harmful because it is bound by various molecules, rendering it non-reactive in terms of redox activity. For example, iron circulates within the plasma bound to transferrin, facilitating its cellular uptake via endocytosis upon binding to transferrin receptor 1 (TFR1). However, in cases of iron overload, the plasma iron levels may exceed the binding capacity of transferrin, leading to the presence of iron not bound to transferrin, commonly referred to as "non-transferrin-bound iron" or "NTBI." This form of iron is characterized by its high redox activity and can induce oxidative damage to various cells and organs by generating reactive oxygen species (ROS) [2][9]. As reviewed by Nakamura et al., iron-mediated reactive oxygen species (ROS) are known to induce various types of cell death, including apoptosis, necroptosis, ferroptosis, and pyroptosis [10].

Research indicates that iron accumulation in thalassemia patients first occurs in the liver [11]. At the cellular level, the uptake of NTBI into cells is facilitated by one or more membrane proteins collectively referred to as NTBI transporters. Included among these are divalent metal transporter 1 (DMT1) and ZRT/IRT-like protein 14 (ZIP14). DMT1 is the principal iron transporter in the duodenum, which also plays a role in transferrin-mediated iron transport [9]. Moreover, research by Shindo et al. demonstrates that DMT1 can also be expressed on the plasma membrane and plays a role in the cellular uptake of NTBI into hepatocytes through a pathway distinct from that mediated by transferrin [12]. Meanwhile the other NTBI transporter, ZIP14, is predominantly expressed in organs prone to iron accumulation, namely the liver, pancreas, and heart, where iron-related pathologies frequently manifest. These findings imply a significant role for ZIP14 in mediating NTBI uptake in these tissues [9]. The research conducted by Jenkitkasemwong et al. substantiates that ZIP14 is essential for the uptake of iron into hepatocytes and acts as a primary NTBI transporter in the liver, playing a crucial role in the development of iron overload conditions in cases of hemochromatosis [13].

To prevent iron accumulation, patients with thalassemia are treated with iron chelation therapy. Currently available iron chelators include deferoxamine, deferasirox, and deferiprone. However, the use of these iron chelators faces several challenges, including inconsistent availability, high cost, and side effects that ultimately affect patient compliance and treatment outcomes [14][15]. Therefore, there is a need for alternative therapies that can address these shortcomings.

Currently, the use of natural substances for treating various diseases, including iron overload, has gained significant interest among researchers. One natural substance that has been studied and shown to reduce iron accumulation in plasma and organs, including the liver and heart, is *Phaleria macrocarpa*. The research shows promising results, with a significant reduction in both plasma and organ iron levels [16][17]. However, previous research has been more focused on the ability of the extract and its active compounds to chelate and remove iron from organs and the body. For example, previous studies have demonstrated that mangiferin, found in the ethanol extract of *Phaleria macrocarpa* fruit, exhibits iron-chelating activity. It has been shown to effectively reduce plasma iron levels and enhance its excretion in urine [18].

The involvement of transporters in the iron uptake process opens up the possibility that inhibiting iron transporters could be a strategic intervention to prevent iron entry and mitigate the consequences of iron overload [13]. To the best of our knowledge, there have been no studies investigating whether compounds present in the ethanol extract of *Phaleria macrocarpa* fruit can prevent iron accumulation in organs by inhibiting the iron transporters DMT1 and ZIP14, which are known to play a crucial role in mediating iron overload, especially in the liver. For this purpose, Computer-Aided Drug Discovery (CADD) methodologies can be employed to accelerate the drug discovery and development process, while also reducing costs and minimizing failure rates in the final stages. One of these methodologies includes molecular docking, which is a computerized approach used to study interactions between small molecules (ligands or drugs) and large molecules (proteins, enzymes, etc.). Docking various compounds from diverse databases can facilitate the screening of a large number of compounds to ultimately identify potential hits. Implementing molecular docking in natural product-based drug discovery can also help explain their traditional uses and identify other potential benefits of these natural products [19-20].

Based on the above description, in this research, we intend to conduct an in-silico exploration using molecular docking to investigate whether the active compounds in the ethanol extract of *Phaleria macrocarpa* fruit have alternative mechanisms for preventing iron overload by interacting with DMT-1 and ZIP-14, the key NTBI transporters. Our hope is that these interactions could potentially inhibit NTBI uptake into the liver, thereby preventing further iron accumulation.

2. Methods

2.1. Homology Modeling and Validation of DMT-1 and ZIP-14 Structures

The structures of the human DMT-1 and ZIP-14 proteins are not available in the Protein Data Bank (<https://www.rcsb.org/>). Therefore, it is necessary to model these proteins to obtain their 3D structures. The modeling was conducted using the homology modeling method via the SWISS-MODEL website (<https://swissmodel.expasy.org/>). The amino acid sequences used for homology modeling were obtained from the NCBI website (<https://www.ncbi.nlm.nih.gov/>). The validity of the resulting models was evaluated based on sequence identity and Ramachandran plot analysis, using tools from SWISS-MODEL and the PROCHECK web server (<https://www.ebi.ac.uk/thornton-srv/software/PROCHECK/>). Models deemed valid were downloaded in the .pdb format.

2.2. Protein and Ligand Preparation

Protein preparation was conducted using AutoDockTools version 1.5.7, which included removing water molecules, adding hydrogen atoms, and applying charges. Subsequently, the protein structure was saved in the .pdbqt format. The ligands used in this study were based on the results of phytochemical screening of ethanol extracts from *Phaleria macrocarpa* fruit from previous research (Table 1) [16]. The 3D structures of the test ligands were downloaded from PubChem (<https://pubchem.ncbi.nlm.nih.gov/>) and then converted to the .pdb format using MarvinSketch software. Further, the number of rotatable bonds was checked, and the structures were stored in the .pdbqt format using AutoDockTools version 1.5.7.

Table 1. Phytochemical Screening Results of Ethanol Extract of *Phaleria macrocarpa* Fruit[16]

No.	Active Compounds
1.	6-Hydroxykaempferol-3-O-Glucoside
2.	Adenine
3.	Apigenin-7-O-Beta-D-Glucuronopyranoside
4.	Arecatannin A2
5.	Cirsimaritin
6.	Epigallocatechin-3-O-Gallate
7.	Evoxidine
8.	Flazin
9.	Gardenin C
10.	Gardenin E
11.	Gentiatibetine
12.	Guanine
13.	Isomangiferin
14.	Isoschaftoside
15.	Kaempferol-7-O-Alpha-L-Arabinofuranoside
16.	Neomangiferin
17.	Patuletin-7-O-[6"-(2-Methylbutyryl)]-Glucoside
18.	Trigonelline
19.	Yuankanin
20.	1,7-Dimethoxy-2,3-Methylenedioxyxanthone
21.	5,7,8,3',4'-Pentamethoxyflavone
22.	6'-O-Galloyl-Homoarbutin
23.	Acacetin-7-O-(6"-O-Acetyl)-Beta-D-Glucopyranoside
24.	Eupafolin
25.	Kaempferol-3-O-Alpha-L-Arabinoside
26.	Khellol-Beta-D-Glucoside
27.	Naringenin-4'-7-Dimethyl Ether
28.	Taxifolin-3-O-Beta-D-Glucopyranoside
29.	Wogonoside

2.3 Determination of Binding Site Locations for DMT-1 and ZIP-14 Proteins

To date, no 3D structures of human DMT-1 and ZIP-14 proteins, either uncomplexed or complexed with a native ligand, are available in the Protein Data Bank. Therefore, the binding site locations have been identified through literature review. DMT-1 is known to possess a substrate binding site in the central region of the protein. This site is formed by the amino acid residues aspartate and asparagine located on α -helix 1 and the amino acid residue methionine on α -helix 6, which acts as a soft ligand capable of coordinating with transition metal ions [21- 22].

According to the study by Anantram et al., the key amino acid residues involved in iron binding within the human DMT-1 model include Val263, Thr112, Leu118, Val114, Leu304, His267, Asp86, Asn89, and Met265 [22]. Meanwhile, the metal binding site of ZIP-14 is known to be located within the intramembrane region, forming a pore structure. The motif EEXPHEXGD in ZIP-14 is recognized as crucial for the metal transport process. Research by Dawson, using a homology modeling approach,

predicts that the key amino acid residues involved in the metal binding site of human ZIP-14 protein are Glu376, Glu377, His380, His347, Asn348, and Asp351 [23]. Subsequently, the locations of these amino acid residues are used as references for manually determining the coordinates for molecular docking by adjusting the grid box to encompass all the amino acid residues involved in iron binding and transport.

2.4 Molecular Docking and Interaction Visualization

Molecular docking was performed using AutoDockTools-1.5.7 software. The grid box size was set to 60x60x60, except for the test ligand Arecatannin, which used an 80x80x80 grid box due to its larger molecular size. The x, y, z coordinates were adjusted based on the binding site location as reported in the literature. Docking parameters followed the default settings of the application. The binding energy between the ligand and the protein was recorded in a table and sorted from the lowest to the highest values. Visualization of interactions was carried out using LigPlot+ software version 2.2. The amino acid residues interacting with the ligand were then recorded in a table. The complete methodology employed in this study is concisely summarized in Figure 1.

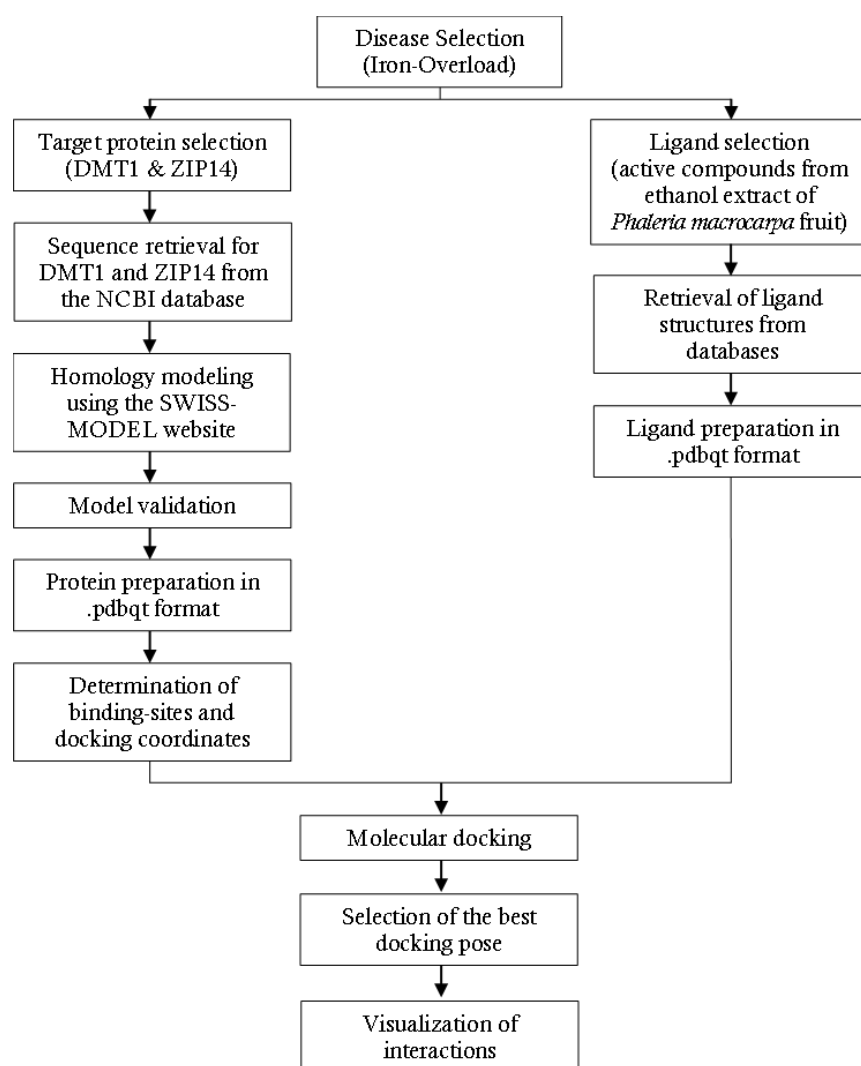


Figure 1. Schematic Diagram for the Homology Modelling and Molecular Docking Process

3. Results and Discussion

3.1 Homology Modeling and Validation of DMT-1 and ZIP-14 Structures

Three-dimensional structures of the DMT-1 and ZIP-14 proteins for molecular docking procedures were obtained through homology modeling. The resulting DMT-1 model (Figure 2a) has a sequence identity of 98.91% with the template. The Ramachandran plot analysis shows that 90.7% of the amino acid residues are in the most favored region, 7.6% in the additional allowed region, 0.6% in the generously allowed region, and 1% in the disallowed region (Figure 2b). Meanwhile, the generated ZIP-14 model (Figure 3a) has a sequence identity of 95.14% with the template. The Ramachandran plot analysis indicates that 84.4% of the amino acid residues are in the most favored region, 13.3% in the additional allowed region, 1.7% in the generously allowed region, and 0.7% in the disallowed region (Figure 3b).

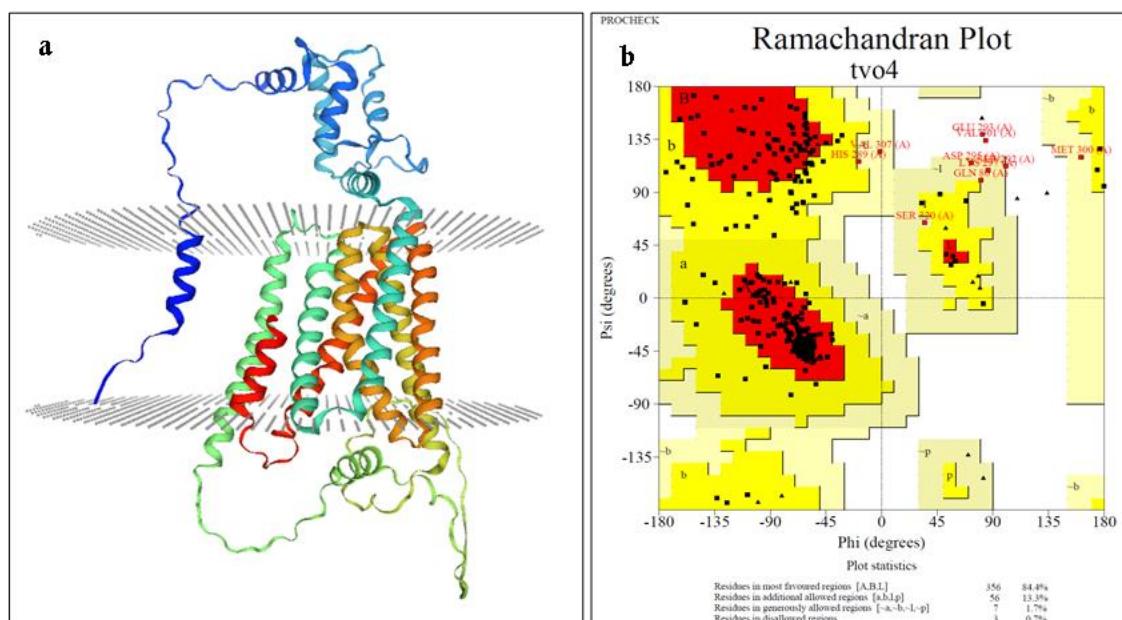


Figure 2. Visualization of the DMT-1 Model Predicted by SwissModel (a) and Structure Validation of DMT-1 Using the Ramachandran Plot (b)

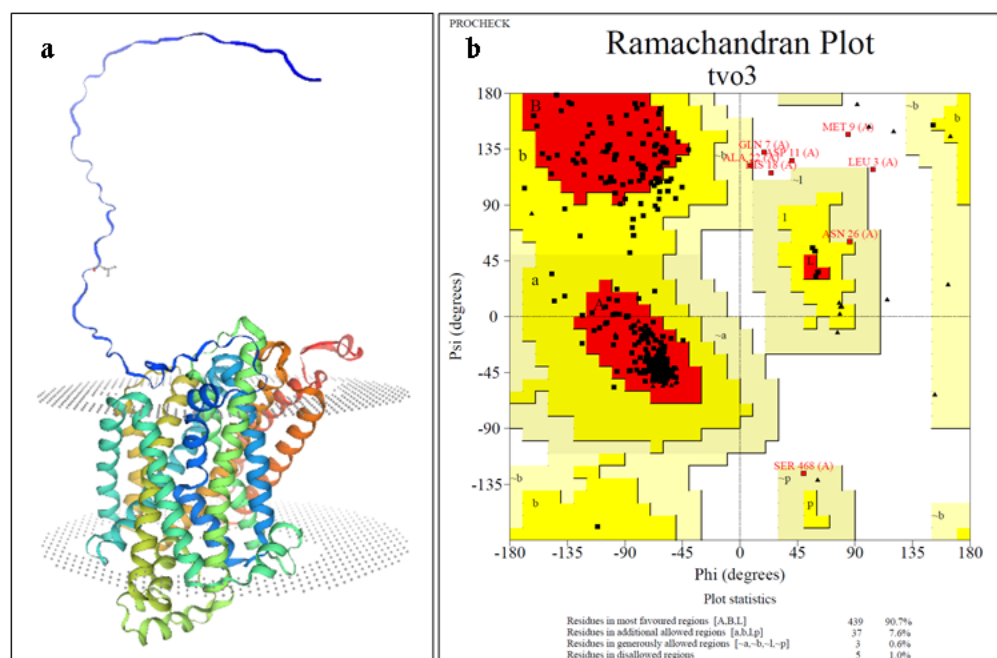


Figure 3. Visualization of the ZIP-14 Model Predicted by SwissModel (a) and Structure Validation of ZIP-14 Using the Ramachandran Plot (b)

Homology modeling is a method used to predict the 3D structures of proteins based on their amino acid sequences, utilizing knowledge gained from structurally similar proteins. This approach relies on two fundamental principles: the primary sequence of amino acids determines the protein's 3D structure, and the 3D structure of a protein is conserved in relation to its primary sequence [20][24-25]. Homology modeling is applicable to protein targets with a sequence identity above 25% [25]. The DMT-1 and ZIP-14 models used in this study have high sequence identities relative to their templates, at 98.91% for DMT-1 and 95.14% for ZIP-14, thereby exceeding the required cut-off value for reliable modeling.

While the models satisfy the criteria for sequence identity, it is imperative to further evaluate the validity of models produced via homology modeling. The Ramachandran plot can serve this purpose. The Ramachandran plot analyzes the backbone dihedral angles ϕ (phi) and ψ (psi), which describe the rotations of the N—C α and C α —C bonds in the polypeptide chain, respectively. These torsion angles dictate the conformation of each residue and the peptide chain. However, certain combinations of these angles can cause atoms to come into close contact, resulting in steric clashes. The Ramachandran plot identifies the permissible torsional angles of the peptide backbone, thereby evaluating the quality of the protein model [26].

A high-quality model should exhibit a distribution where a significant proportion of amino acid residues (at least 90%) are located within the favorable and allowed regions [27-28]. The Ramachandran plot analysis for the models of DMT-1 and ZIP-14 used in this study indicates that more than 90% of the amino acid residues are located in the most favorable and allowed regions. In other words, the DMT-1 and ZIP-14 models obtained from homology modeling demonstrate structurally plausible and high-quality conformations, making them suitable for subsequent molecular docking processes.

3.2 Binding-Site Location and Molecular Docking Coordinates

Figure 4 illustrates the location of the amino acid residues involved in the iron binding and transport processes in the DMT-1 protein as identified from the literature (a), along with the position of the gridbox that will be used for molecular docking (b). The coordinates x, y, z for the molecular docking of the DMT-1 protein is -3.455, 2.041, and 3.070, respectively. Figure 5 illustrates the location of the amino acid residues involved in the iron binding and transport processes in the ZIP-14 protein as identified from the literature (a), along with the position of the grid box that will be used for molecular docking (b). The coordinates x, y, z for the molecular docking of the ZIP-14 protein is -3.115, 4.585, and 5.610.

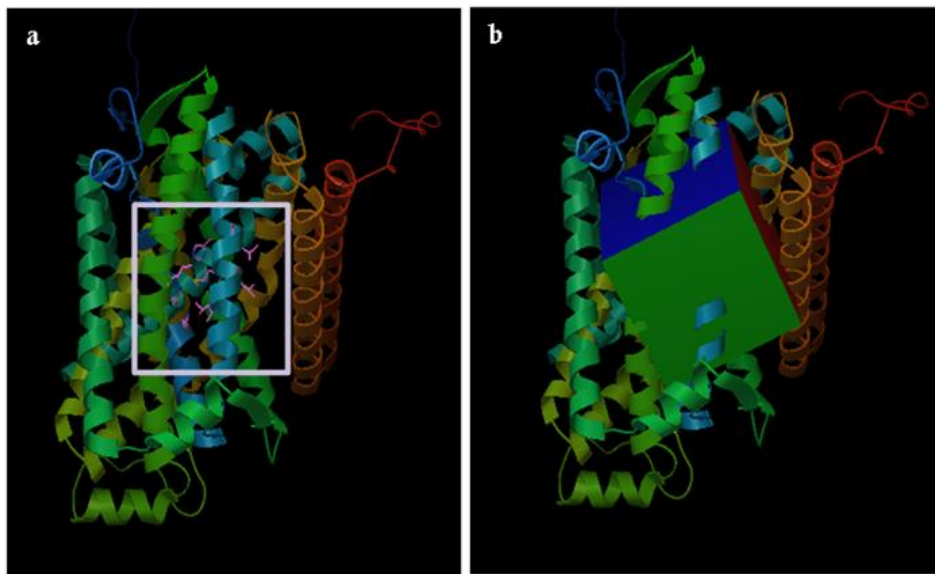


Figure 4. Location of amino acid residues for iron binding (a) and gridbox (b) for molecular docking of the DMT-1 protein.

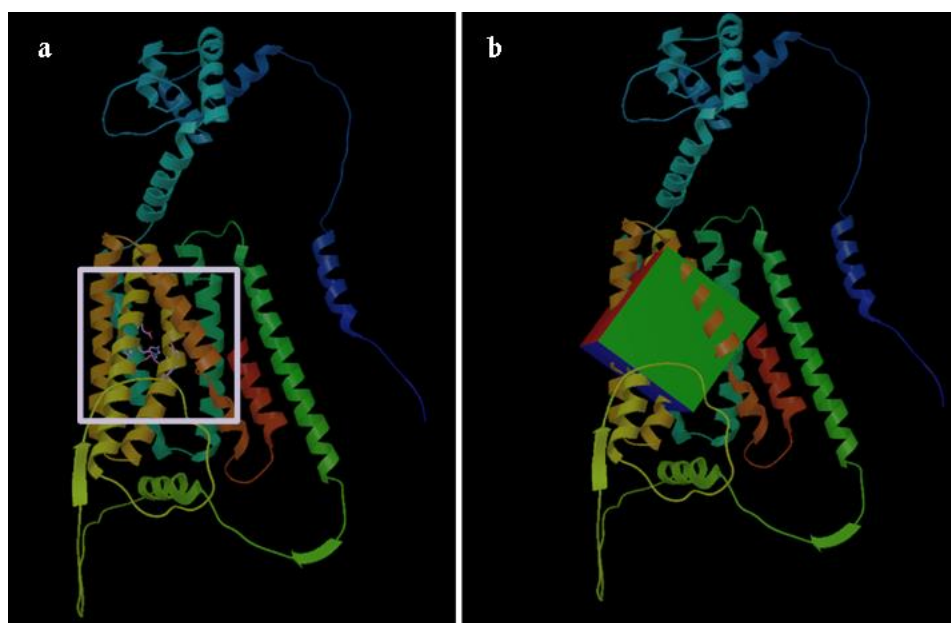


Figure 5. Location of amino acid residues for iron binding (a) and gridbox (b) for molecular docking of the ZIP-14 protein.

3.3 Molecular Docking, Analysis, and Visualization of Protein-Ligand Interaction

The binding energies between the proteins DMT-1 and ZIP-14 with each ligand are listed in Tables 2 and 3. According to Table 2, the three active compounds from the ethanol extract of *Phaleria macrocarpa* fruit showing the lowest binding energies with DMT-1 are patuletin-7-O-[6''-(2-methylbutyryl)]-glucoside, naringenin-4'-7-dimethyl ether, and 5,7,8,3',4'-pentamethoxyflavone, with binding energy values of -6.00 kcal/mol, -5.58 kcal/mol, and -5.35 kcal/mol respectively. As per Table 3, the three active compounds from the ethanol extract of *Phaleria macrocarpa* fruit showing the lowest binding energies with ZIP-14 are 6'-O-galloyl-homoarbutin, patuletin-7-O-[6''-(2-methylbutyryl)]-glucoside and guanine, with binding energy values of -8.11 kcal/mol, -6.98 kcal/mol, and -6.47 kcal/mol respectively.

Table 2. Molecular Docking Results for DMT-1 Protein with Active Constituents of Ethanol Extract of *Phaleria macrocarpa* Fruit

No.	Ligands	Binding Energy (kcal/mol)
1.	Patuletin-7-O-[6''-(2-methylbutyryl)]-glucoside	-6.00
2.	Naringenin-4'-7-dimethyl ether	-5.58
3.	5,7,8,3',4'-pentamethoxyflavone	-5.35
4.	6'-O-galloyl-homoarbutin	-5.20
5.	1,7-dimethoxy-2,3-methylenedioxyxanthone	-4.72
6.	Cirsimaritin	-4.56
7.	Gentiatibetine	-4.49
8.	Evoxidine	-4.47
9.	Kaempferol-7-O-alpha-L-arabinofuranoside	-4.35
10.	Adenine	-4.09
11.	Gardenin c	-4.02
12.	Gardenin e	-3.93
13.	Eupafolin	-3.84
14.	Flazin	-3.67
15.	Trigonelline	-3.65
16.	Guanine	-3.35
17.	Isomangiferin	-1.72
18.	Kaempferol-3-O-alpha-L-arabinoside	-1.44
19.	Khellol-beta-D-glucoside	-0.44
20.	Wogonoside	+0.57
21.	Taxifolin-3-o-beta-d-glucopyranoside	+0.79
22.	Apigenin-7-O-beta-D-glucuronopyranoside	+3.38
23.	6-hydroxykaempferol-3-o-glucoside	+6.91
24.	Acacetin-7-O-(6''-O-acetyl)-beta-D-glucopyranoside	+7.81
25.	Epigallocatechin-3-O-gallate	+9.53
26.	Yuankanin	+14.45
27.	Arecatannin A2	+15.78
28.	Isoschaftoside	+72.04
29.	Neomangiferin	+73.61

Table 3. Molecular Docking Results for ZIP-14 Protein with Active Constituents of Ethanol Extract of *Phaleria macrocarpa* Fruit

No.	Ligands	Binding Energy (kcal/mol)
1.	6'-O-galloyl-homoarbutin	-8.11
2.	Patuletin-7-O-[6''-(2-methylbutyryl)]-glucoside	-6.98
3.	Guanine	-6.47
4.	1,7-dimethoxy-2,3-methylenedioxyxanthone	-6.10
5.	Naringenin-4'-7-dimethyl ether	-6.08
6.	Arecatannin A2	-5.99
7.	Acacetin-7-O-(6''-O-acetyl)-beta-D-glucopyranoside	-5.73
8.	Eupafolin	-5.61
9.	Kaempferol-7-O-alpha-L-arabinofuranoside	-5.45
10.	Evoxidine	-5.44
11.	Cirsimaritin	-5.37
12.	Khellol-beta-D-glucoside	-5.32
13.	5,7,8,3',4'-pentamethoxyflavone	-5.28
14.	Gardenin e	-4.98
15.	Gentiatibetine	-4.86
16.	Kaempferol-3-O-alpha-L-arabinoside	-4.76
17.	Isomangiferin	-4.74
18.	Flazin	-4.68
19.	Epigallocatechin-3-O-gallate	-4.25
20.	Adenine	-4.11
21.	Wogonoside	-3.63
22.	Gardenin c	-3.53
23.	6-hydroxykaempferol-3-o-glucoside	-3.05
24.	Taxifolin-3-o-beta-d-glucopyranoside	-2.73
25.	Trigonelline	-2.48
26.	Apigenin-7-O-beta-D-glucuronopyranoside	-2.01
27.	Yuankanin	-0.73
28.	Neomangiferin	+3.40
29.	Isoschaftoside	+7.97

Analysis and visualization of interactions were conducted on the three ligand-protein complexes with the lowest binding energies. The complexes analyzed include the DMT-1 complex with patuletin-7-O-[6''-(2-methylbutyryl)]-glucoside, naringenin-4'-7-dimethyl ether, and 5,7,8,3',4'-pentamethoxyflavone (Figure 6), as well as the ZIP-14 complex with 6'-O-galloyl-homoarbutin, patuletin-7-O-[6''-(2-methylbutyryl)]-glucoside, and guanine (Figure 7). The amino acid residues involved in the ligand-protein interactions are listed in Tables 4 and 5.

The interactions between DMT-1 amino acid residues and the selected test compounds (patuletin-7-O-[6''-(2-methylbutyryl)]-glucoside, naringenin-4'-7-dimethyl ether, and 5,7,8,3',4'-pentamethoxyflavone) consist solely of hydrophobic interactions, with no hydrogen bonds present. On the other hand, the interactions between ZIP-14 amino acid residues and 6'-O-galloyl-homoarbutin and patuletin-7-O-[6''-(2-methylbutyryl)]-glucoside involve a single hydrogen bond, while interactions with guanine include three hydrogen bonds, with the remainder being hydrophobic interactions.

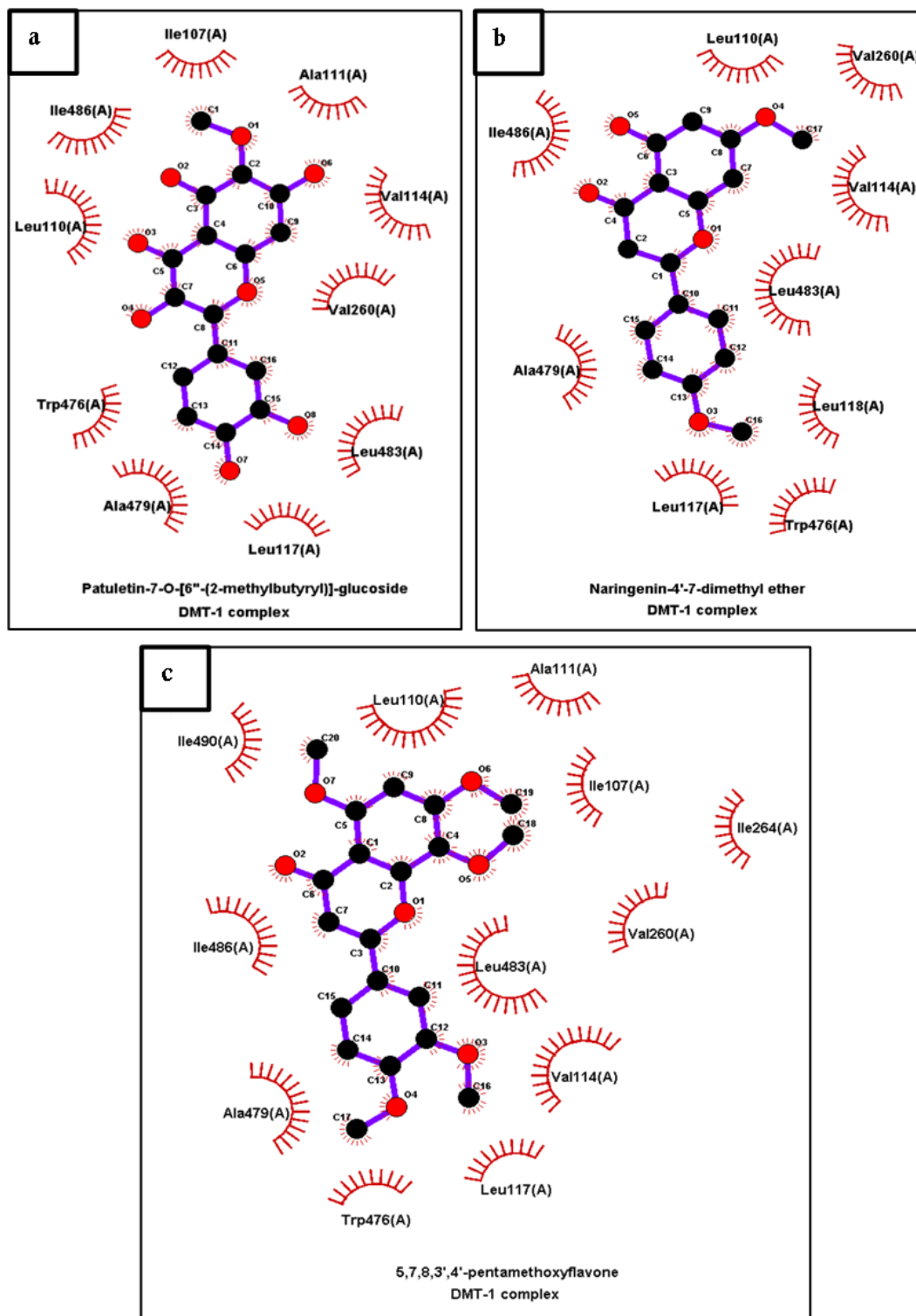


Figure 6. Interaction Visualizations between DMT-1 and patuletin-7-O-[6''-(2-methylbutyryl)]-glucoside (a), naringenin-4'-7-dimethyl ether (b), and 5,7,8,3',4'-pentamethoxyflavone (c).

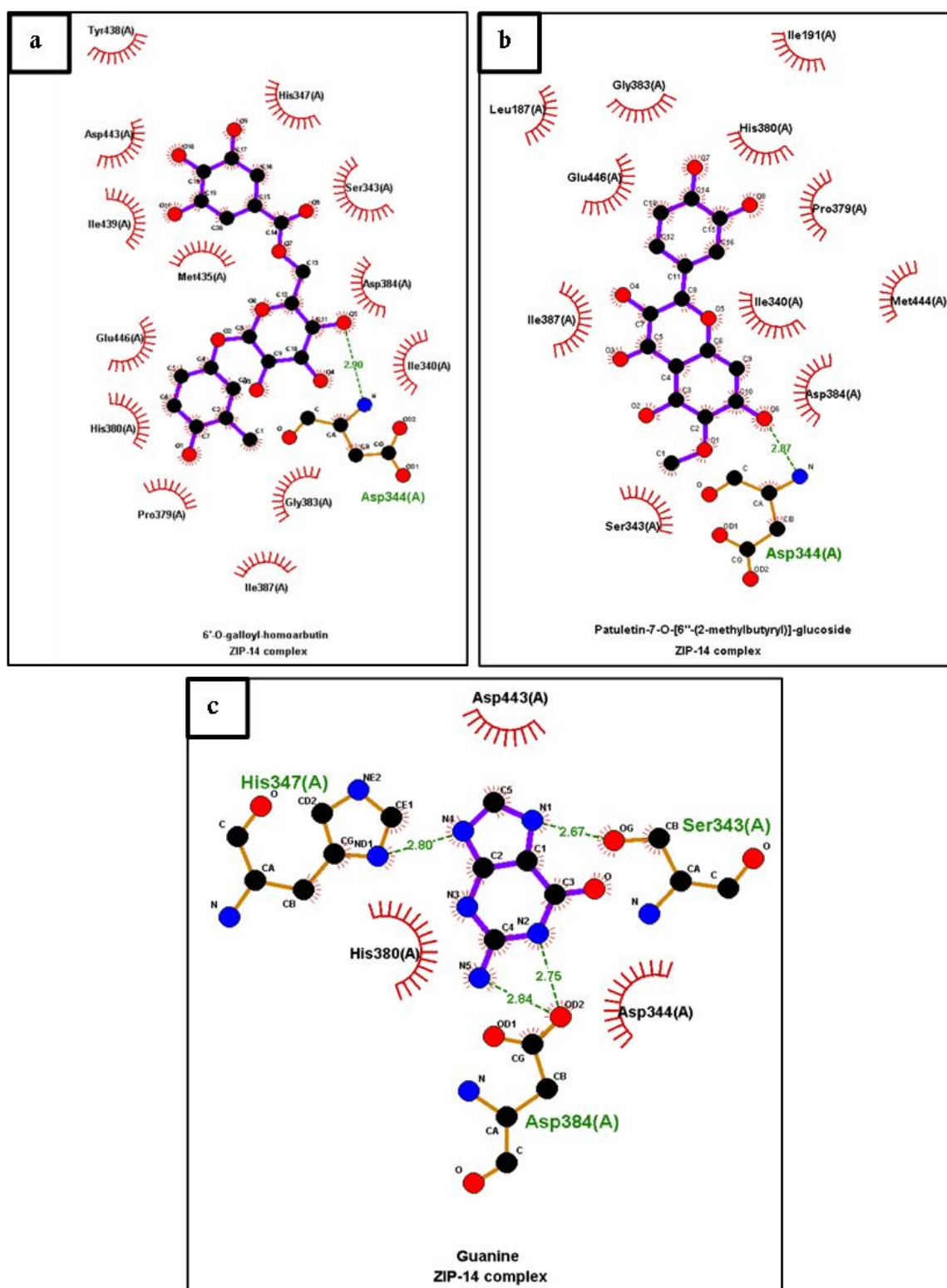


Figure 7. Interaction Visualizations between ZIP-14 and 6'-O-galloyl-homoarbutin (a), patuletin-7-O-[6''-(2-methylbutyryl)]-glucoside (b), and guanine (c).

Table 4. Amino Acid Residues Involved in Ligand-Protein Interactions with DMT-1

No.	Patuletin-7-O-[6''-(2-methylbutyryl)]-glucoside	Naringenin-4'-7-dimethyl ether	5,7,8,3',4'-Pentamethoxyflavone
1.	Ile107	Leu110	Ile107
2.	Leu110	Val114	Leu110
3.	Ala111	Leu117	Ala111
4.	Val114	Leu118	Val114
5.	Leu117	Val260	Leu117
6.	Val260	Trp476	Val260
7.	Trp476	Ala479	Ile264
8.	Ala479	Leu483	Trp476
9.	Leu483	Ile486	Ala479
10.	Ile486	-	Leu483
11.	-	-	Ile486
12.	-	-	Ile490

Table 5. Amino Acid Residues Involved in Ligand-Protein Interactions with ZIP-14

No.	6'-O-galloyl-homoarbutin	Patuletin-7-O-[6''-(2-methylbutyryl)]-glucoside	Guanine
1	Ile340	Leu187	Asp344
2	Ser343	Ile191	Ser343*
3	Asp344*	Ile340	His347*
4	His347	Ser343	His380
5	Pro379	Asp344*	Asp384*
6	His380	Pro379	Asp443
7	Gly383	His380	-
8	Asp384	Gly383	-
9	Ile387	Asp384	-
10	Met435	Ile387	-
11	Tyr438	Met444	-
12	Ile439	Glu446	-
13	Asp443	-	-
14	Glu446	-	-

Note: *Hydrogen bonds

The interaction between the ligands and target proteins (DMT1 and ZIP14) was analyzed using a molecular docking approach. This method estimates the ligand's binding affinity to form a stable complex with the protein by determining the preferred orientation that minimizes the free binding energy [20]. Negative binding energy (ΔE) indicates that the complex formation process involves the release of energy, thereby demonstrating stability. In other words, the lower the binding energy, the higher the affinity and stability of the ligand-protein complex [29-30]. Generally, a binding energy lower than -5.00 kcal/mol indicates a strong affinity between the ligand and the protein [31]. The results of molecular docking of active compounds from the ethanol extract of *Phaleria macrocarpa* fruit in this study indicate that four compounds were able to interact with DMT-1 and fourteen compounds were able to interact with ZIP-14, each with a binding energy below -5.00 kcal/mol.

Hydrogen bonds are essential for molecular recognition and binding specificity in docking processes. They contribute to the stabilization of protein-ligand complexes by forming strong and directional interactions [32-33]. The increase in such directional interactions enhances binding

specificity, thereby improving a compound's selectivity towards its target [34]. Conversely, hydrophobic interactions, which are non-covalent bonds resulting from the interaction of non-polar molecules, contribute to the high affinity of compounds and provide attractive forces that stabilize the complex [34]. In this research, we performed an interaction analysis between each protein and the top three compounds identified based on their minimal binding energies. The analysis revealed that the interactions of DMT-1 with the top three active compounds from the ethanol extract of *Phaleria macrocarpa* comprised exclusively hydrophobic interactions. Conversely, the interactions with ZIP-14 included at least one hydrogen bond.

The results of the interaction analysis suggest that the active compounds from the ethanol extract of *Phaleria macrocarpa* fruit demonstrates more favorable interactions with ZIP14 compared to DMT1. This is indicated by a greater number of compounds capable of interacting with lower binding energies and the presence of hydrogen bonds. This finding is favorable, as research indicates that ZIP-14 plays a more significant role in causing iron overload, whereas DMT-1 has a minor role [13]. Therefore, inhibiting ZIP-14 is likely to have a more substantial impact on preventing iron overload in organs, particularly the liver. Overall, these findings suggest that the ethanol extract of *Phaleria macrocarpa* fruit may have an alternative mechanism for reducing iron accumulation in the liver by interacting with iron transporters, potentially exerting an inhibitory effect.

4. Conclusion

The in-silico results of this study indicate that various active compounds from the ethanol extract of *Phaleria macrocarpa* fruit can interact with DMT-1 and ZIP-14, which are iron transporters involved in the pathogenesis of iron-overload. The choice of docking coordinates was based on literature indicating an inhibitory effect upon ligand binding at these sites. Consequently, interactions between the active compounds of the ethanol extract of *Phaleria macrocarpa* and DMT-1 and ZIP-14 are expected to induce inhibitory effects that could prevent iron-overload. However, it is important to note that molecular docking only provides information on the binding affinity of a ligand at a protein's binding site. Conclusions about whether the ligand acts as an agonist or inhibitor can only be validated through bioassays.

Another limitation of the molecular docking performed in this study is the assumption that proteins are rigid, except for certain amino acid residues. In reality, when ligands and proteins interact, both adjust their conformations to each other. Therefore, it is recommended that research continues to the stage of molecular dynamics simulations, which more closely resemble actual conditions. These simulations will predict the movement of atoms over time based on the general principles of physics governing inter-atomic interactions, thus providing insights into conformational changes and ligand binding dynamics.

References

- [1] Zeidan, R.S., Martenson, M., Tamargo, J.A., McLaren, C., Ezzati, A., Lin, Y., et al. (2024). Iron homeostasis in older adults: balancing nutritional requirements and health risks. *Journal of Nutrition, Health and Aging*, 28 (5), 1–12.
- [2] Katsarou, A. and Pantopoulos, K. (2020). Basics and principles of cellular and systemic iron homeostasis. *Molecular Aspects of Medicine*, 75 (May), 100866.
- [3] dos Santos, L., Bertoli, S.R., Ávila, R.A., and Marques, V.B. (2022). Iron overload, oxidative stress and vascular dysfunction: Evidences from clinical studies and animal models. *Biochimica et Biophysica Acta - General Subjects*, 1866 (9), 1–12.
- [4] Pan, L., Xie, Y., Yin, X., Huang, Y., Yang, G., Li, C., et al. (2023). Oxidative Stress Damage of Iron Overload on Bone Marrow Erythropoiesis, Heart and Liver in Non-Transfusion Dependent Thalassemia. *Blood*, 142 5245.

- [5] Dhanya, R., Sedai, A., Ankita, K., Parmar, L., Agarwal, R.K., Hegde, S., et al. (2020). Life expectancy and risk factors for early death in patients with severe thalassemia syndromes in South India. *Blood Advances*, 4 (7), 1448–1457.
- [6] Tantiworawit, A., Kamolsripat, T., Piriyaikhuntorn, P., Rattanathammethee, T., Hantrakool, S., Chai-Adisaksopha, C., et al. (2024). Survival and causes of death in patients with alpha and beta-thalassemia in Northern Thailand. *Annals of Medicine*, 56 (1), 1–8.
- [7] Ganz, T. and Nemeth, E. (2023). Pathogenic Mechanisms in Thalassemia II: Iron Overload. *Hematology/Oncology Clinics of North America*, 37 (2), 353–363.
- [8] Koppenol, W.H. and Hider, R.H. (2019). Iron and redox cycling. Do's and don'ts. *Free Radical Biology and Medicine*, 133 3–10.
- [9] Knutson, M.D. (2019). Non-transferrin-bound iron transporters. *Free Radical Biology and Medicine*, 133 (August 2018), 101–111.
- [10] Nakamura, T., Naguro, I., and Ichijo, H. (2019). Iron homeostasis and iron-regulated ROS in cell death, senescence and human diseases. *Biochimica et Biophysica Acta - General Subjects*, 1863 (9), 1398–1409.
- [11] Chapchap, E.C., Silva, M.M.A., de Assis, R.A., Kerbauy, L.N., Diniz, M. da S., Rosemberg, L.A., et al. (2023). Cardiac iron overload evaluation in thalassaemic patients using T2* magnetic resonance imaging following chelation therapy: a multicentre cross-sectional study. *Hematology, Transfusion and Cell Therapy*, 45 (1), 7–15.
- [12] Shindo, M., Torimoto, Y., Saito, H., Motomura, W., Ikuta, K., Sato, K., et al. (2006). Functional role of DMT1 in transferrin-independent iron uptake by human hepatocyte and hepatocellular carcinoma cell, HLF. *Hepatology Research*, 35 (3), 152–162.
- [13] Jenkitkasemwong, S., Wang, C.Y., Coffey, R., Zhang, W., Chan, A., Biel, T., et al. (2015). SLC39A14 Is Required for the Development of Hepatocellular Iron Overload in Murine Models of Hereditary Hemochromatosis. *Cell Metabolism*, 22 (1), 138–150.
- [14] Njeim, R., Naouss, B., Bou-Fakhredin, R., Haddad, A., and Taher, A. (2024). Unmet needs in β -thalassemia and the evolving treatment landscape. *Transfusion Clinique et Biologique*, 31 (1), 48–55.
- [15] Chong, C.C., Redzuan, A.M., Sathar, J., and Makmor-Bakry, M. (2021). Patient Perspective on Iron Chelation Therapy: Barriers and Facilitators of Medication Adherence. *Journal of Patient Experience*, 8.
- [16] Lindayana, Kusmardi, and Estuningtyas, A. (2022). The Effect of Ethanol Extract of *Phaleria Macrocarpa* Fruit in An Iron-Overloaded Rat Heart, Universitas Indonesia, 2022.
- [17] Verna, F. Dela (2021). The hepatoprotective effect of mahkota dewa (*Phaleria macrocarpa*) fruit ethanol extract in iron-overload rats via iron chelating mechanism., University of Indonesia, 2021.
- [18] Estuningtyas, A., Wahyuni, T., Wahidiyat, P.A., Poerwaningsih, E.H., and Freisleben, H.J. (2019). Mangiferin and mangiferin-containing leaf extract from *Mangifera foetida* L for therapeutic attenuation of experimentally induced iron overload in a rat model. *Journal of HerbMed Pharmacology*, 8 (1), 21–27.
- [19] Asiamah, I., Obiri, S.A., Tamekloe, W., Armah, F.A., and Borquaye, L.S. (2023). Applications of molecular docking in natural products-based drug discovery. *Scientific African*, 20.
- [20] Shah, M., Patel, M., Shah, M., Patel, M., and Prajapati, M. (2024). Computational transformation in drug discovery: A comprehensive study on molecular docking and quantitative structure activity relationship (QSAR). *Intelligent Pharmacy*, 2024.

-
- [21] Manatschal, C., Pujol-Giménez, J., Poirier, M., Reymond, J.L., Hediger, M.A., and Dutzler, R. (2019). Mechanistic basis of the inhibition of slc11/nramp-mediated metal ion transport by bis-isothiourea substituted compounds. *ELife*, 8.
- [22] Anantram, A., Janve, M., Degani, M., Singhal, R., and Kundaikar, H. (2018). Homology modelling of human divalent metal transporter (DMT): Molecular docking and dynamic simulations for duodenal iron transport. *Journal of Molecular Graphics and Modelling*, 85 145–152.
- [23] Dawson, C.N. (2022). Disease-Causing Mutations in The Human Metal Ion Transporter ZIP14 Alter Its Structure, Ion Uptake Function and Trafficking, 2022.
- [24] Hameduh, T., Haddad, Y., Adam, V., and Heger, Z. (2020). Homology modeling in the time of collective and artificial intelligence. *Computational and Structural Biotechnology Journal*, 18 3494–3506.
- [25] Jisna, V.A. and Jayaraj, P.B. (2021). Protein Structure Prediction: Conventional and Deep Learning Perspectives. *Protein Journal*, 40 (4), 522–544.
- [26] Chang, Y., Hawkins, B.A., Du, J.J., Groundwater, P.W., Hibbs, D.E., and Lai, F. (2023). A Guide to In Silico Drug Design. *Pharmaceutics*, 15 (49), 1–52.
- [27] Singh, P., Shaikh, S., Gupta, S., and Gupta, R. (2023). In-silico development of multi-epitope subunit vaccine against lymphatic filariasis. *Journal of Biomolecular Structure and Dynamics*, .
- [28] Mir, A., Song, Y., Lee, H., Khanahmad, H., Khorram, E., Nasiri, J., et al. (2023). Whole exome sequencing revealed variants in four genes underlying X-linked intellectual disability in four Iranian families: novel deleterious variants and clinical features with the review of literature. *BMC Medical Genomics*, 16 (239), 1–20.
- [29] Li, T., Guo, R., Zong, Q., and Ling, G. (2022). Application of molecular docking in elaborating molecular mechanisms and interactions of supramolecular cyclodextrin. *Carbohydrate Polymers*, 276.
- [30] García-Ortegón, M., Simm, G.N.C., Tripp, A.J., Hernández-Lobato, J.M., Bender, A., and Bacallado, S. (2022). DOCKSTRING: Easy Molecular Docking Yields Better Benchmarks for Ligand Design. *Journal of Chemical Information and Modeling*, 62 (15), 3486–3502.
- [31] Ma, X., Pan, B., Wang, L., Feng, Z., and Peng, C. (2023). Network pharmacology and molecular docking elucidate potential mechanisms of *Eucommia ulmoides* in hepatic ischemia–reperfusion injury. *Scientific Reports*, 13 (20716), 1–14.
- [32] Olugbogi, E.A., Arobadade, O.A., Bodun, D.S., Omoseeye, S.D., Omirin, E.S., Fapohunda, O., et al. (2023). Identification of apposite antagonist for androgen receptor in prostate cancer: an in silico study of fenugreek compounds. *Journal of Biomolecular Structure and Dynamics*.
- [33] Madushanka, A., Moura, R.T., Verma, N., and Kraka, E. (2023). Quantum Mechanical Assessment of Protein–Ligand Hydrogen Bond Strength Patterns: Insights from Semiempirical Tight-Binding and Local Vibrational Mode Theory. *International Journal of Molecular Sciences*, 24 (7).
- [34] Girdhar, N., Yadav, V., Kumari, N., Subbarao, N., and Krishnamachari, A. (2024). Insilico screening to identify novel inhibitors targeting 30S ribosomal protein S12 in meningitis-causing organism ‘*Elizabethkingia meningoseptica*.’ *Journal of Biomolecular Structure and Dynamics*.